A canonical numerical experiment to study detonation initiation from colliding subsonic auto-ignition waves

S. Taileb, G. Farag, Vincent Robin, A. Chinnayya

A canonical numerical experiment to study detonation initiation from colliding subsonic auto-ignition waves

S. Taileb,[1, a)] G. Farag,[1] V. Robin,[1] and A. Chinnayya[1]
Institut PPRIME - UPR 3346, CNRS - ISAE-ENSMA - Université de Poitiers, Téléport 2, 1 Av. Clément Ader, Chasseneuil-du-Poitou, 86360, France

(*Electronic mail: vincent.robin@isae-ensma.fr)

(Dated: 5 June 2023)

The collision of two subsonic auto-ignition fronts with initial constant velocity was found to transit to detonation only when the collision angle was acute. The interaction of the reactive phase wave with inert hot layers constituted a singularity providing a continuous source of vorticity due to barocline effect. For an acute angle, this singularity that propagated at supersonic speed, induced oblique pressure waves, of which resonance, due to the reactivity gradient geometry, near the center of the channel in the fresh gases accelerated the reactive wave fronts until transition to detonation. The numerical results of the present study, even if based on drastic assumptions were at least in good qualitative consistency with experiments. The geometry of the reactivity gradients can thus provide another seed for the coupling between gasdynamics and heat release. Continuous pressure fluctuations and oblique shocks coming from vorticity sources and sheets from barocline effects can considerably enhance this transition. This path to transition could be complementary to that invoking mixing burning within premixed non-planar turbulent flame brush.

I. INTRODUCTION

The transition from a subsonic deflagration to a supersonic detonation wave can be achieved through different scenarios, involving interactions of flames with shocks, boundary layers, instabilities or turbulence. These issues have been extensively studied over the past decades, since at least the work of Meyer, Urtiew, and Oppenheim [1] and are still the subject of numerous recent works[2–5]. The physics of Deflagration to Detonation Transition (DDT) is extremely rich (see seminal review of Oran and Gamezo[6] or textbooks[7,8]) and a variety of mechanisms have been revealed in industrial applications, such as engines, mines, and also in natural phenomenon, such as explosions of supernova[9]. The underlying physical mechanisms are responsible for safety hazards issues, the rare detonation or explosions event being to be prevented when handling and storing energetic materials. For propulsion devices, a better understanding is still mandatory to improve the reliability of ignition relying on fast combustion waves[10], such as the rotating detonation engine[11] and the pulsed detonation engine[12]. More recently, in the context of a rapid decrease of greenhouse gas emissions, the expected increase of hydrogen use for conventional combustion system has stressed the focus on pre-ignition and knocking issues observed in spark-ignition engines[13–16]. These undesirable phenomena can considerably limit the thermal efficiency of the devices and can even lead to their destruction.

What emerges from the various and very rich previous studies is that many different mechanisms, namely flame folding, non-uniformity, pressure wave focusing, thermal feedback, hot spot generation, etc., can cause a detonation initiation. It is even highly probable that the initiation of the detonation in practical multidimensional flows results from these sequential or combined effects on the fresh gases. These mechanisms have then to be analyzed separately. In this context, the objective of this work is to improve the understanding of the physical mechanisms preceding a detonation by using a new canonical numerical experiment highlighting the fundamental successive steps of a specific scenario of detonation initiation.

The physical mechanisms triggering a detonation are so intricate that the realizable initiation scenarios are numerous and difficult to classify. We have chosen here to follow Poludnenko et al.[17] where the main means of detonation initiation were sorted into three categories. First, the strong ignition is the result of an initial shock wave strong enough to trigger chemical reactions in a very short time. Second, weak ignition involves the Zel'dovich gradient mechanism[18], which results in a phase wave of auto-ignition in a non-uniform temperature or composition field. Among others, the seminal work of Kapila *et al.* [19] provided a parametric study for a planar configuration and elementary kinetics in a gradient of reactivity. For shallow gradients, the reactive wave was supersonic, with little effect on hydrodynamics. The transition to detonation may occur if the wave decelerated to the Chapman-Jouguet (CJ) speed. For sharper gradients, the speed of the reactive wave was lower but could generate a shock, strong enough to modify the reactivity gradient and to accelerate the reactive wave until the coupling of the leading shock and the reaction wave, see the SWACER (Shock Wave Acceleration due to Coherence Energy Release)[7]. The third means for detonation initiation is DDT. Indeed, a flame propagating by heat and molecular diffusion at constant speed, initially laminar, increases its surface through hydrodynamic instabilities, interactions with turbulence, and/or boundary layers until its propagation speed becomes large enough to trigger a precursor shock. This latter mechanism, enhanced by flow confinement, has been largely studied in tubes where the flame propagates from the closed end of the tube[20,21].

The increase of the flame area is a powerful image to explain the global acceleration of the flame brush before the occurence of the detonation. However, the local mechanisms at hand are not completely described. Two main different ap-

[a)] Present address: Safran Tech, Magny-les-Hameaux, France.

proaches, baring some similarities, coexist to explain how the local flamelets whose internal structures are laminar and speed largely subsonic, can produce a precursor shock.

First, the positive thermal feedback mechanism has been studied in details in recent numerical simulations[22–24] whose theoretical basis was established in the early work of Deshaies and Joulin[25] and whose ideas were discussed as early as in the fifties[26]. The flame acceleration induced compression waves[26], which heated the fresh gases, further accelerating the flame due to shorter induction times and higher temperature of fresh gases, reinforcing the compression waves, and so forth. The latter would build up to steepen into a leading shock and the flame would further accelerated until coupling with the shock to form eventually a detonation wave. Another 1-D model has also been recently proposed to model DDT on the tip of elongated flames in tubes[5] where the back-flow of burnt-gas, pushing the flame-tip, produced a double-feedback mechanism. However, an unanswered question concerns the internal structure of a flame subjected to such thermal feedback. Indeed, the laminar structure, composed of a large diffusion layer and a thin reaction zone, cannot be maintained when the flame becomes very fast.

The second approach involved explosion centers, see reviews of Oran and Gamezo[6], Oran, Chamberlain, and Pekalski[27] and Kapila *et al.*[19]. The compression waves, which focused into shock waves also developed reactivity gradients of composition and temperature, in the neighbourhood locus of these focusing events. If the speed associated with this gradient of self-ignition delays is about the speed of sound[18], the reaction zone and the shock wave may thus couple before transition. This synchronisation also referred to the SWACER mechanism[7,19].

Poludnenko[28] provided a detailed description of self-accelerating turbulent flames in unconfined configurations for which the flame surface increased continuously due to turbulence and then decreased intermittently due to flame collisions. The flow exhibited strong pressure waves and shocks before the generation of hot spots and transition to detonation, when the turbulence intensity increased further[29]. Once the flame speed exceeded a CJ deflagration speed, transition to detonation took place as a catastrophic runaway pressure buildup, the flame motion being in phase with pressure waves. Strong shocks were generated within the turbulent brush in some cases. This mechanism was independent of the turbulent structure of the flame, the combustion regime and the reactive mixture. Very recently, Chambers *et al.*[30] experimentally explored turbulence-induced DDT. Poludnenko also showed that in other cases, the strong shock ran ahead of the flame brush. In configuration with obstacles, Rakotoarison *et al.*[31], Rakotoarison, Pekalski, and Radulescu[32] showed for insensitive mixtures that a strong intensity of turbulence due to shock reflections increased the local speed of the flame closer to the speed of sound. Detonation was then observed in regions where the turbulent flame shape was non-planar.

Whichever approach is retained to explain the local transition mechanism, compression waves that are generated by flame acceleration are involved. These waves either accelerate the flame itself due to the heating of fresh gases (thermal feedback mechanism) or generate a reactivity gradient near the shock or within the flame brush, likely to transit. Moreover, a flame propagating at a speed significantly higher than its laminar speed must have an internal structure that is largely different from its laminar structure. Indeed, in the limit of large velocity and relatively high initial temperature, the convection term dominates over the diffusion term, becoming mainly balanced by reaction. Thus, the flame structure becomes similar to that of an auto-ignition front for large flame speed. The interaction of such spontaneous ignition front with turbulent flow has recently been investigated[33] numerically for high turbulence levels in simple configurations, clearly affecting the above picture.

The canonical numerical experiment proposed here is designed to highlight multi-dimensional effects of the entanglement of laminar auto-ignition fronts and compression waves. The proposed configuration was motivated by Podulenko's[17,28,29,34] and Rakotoarison's[31,32] works, with drastic simplifications.

First, Poludnenko *et al.*[17] and Rakotoarison *et al.*[31] clearly indicated that the non-planarity of the flame could promote compression waves and further transition. However, turbulence was not considered in the present study. Instead, the turbulent flame was replaced with an auto-ignition front with sharp gradient. Then, the collision of two auto-ignition fronts with a prescribed angle was studied in order to simulate the non-planarity aspect. Two cases were investigated: an obtuse and an acute angle. The proposed canonical configuration mimicked the flame collisions and related decrease of the flame area. It remained fairly close to the case of a funnel, whose section was pinched, see Oran and Gamezo[6]. This configuration could also arise from the interaction of a shock wave with a cellular flame, see Yang and Radulescu[35]. One of the most striking experimental evidence of a funnel was that of Fig. 1a of Meyer, Urtiew, and Oppenheim[1]. Kagan, Liberman, and Sivashinsky[36] have also shown that deflagration driven and confined by non-planar hot walls could initiate a detonation. Thus, flame acceleration was induced by both thermal diffusion from walls and pressure wave reflections on walls. The canonical configuration proposed here is semi-confined and the effects of molecular diffusion are neglected.

Second, in order to avoid any effect of wall confinement and computational boundaries, inert layers at high temperature surrounded the reactive layer. Thus, the second thermal feedback[5] was minimized by avoiding wave reflection on walls. The boundaries of the computational domain were fully transmissive.

Third, the ignition front speed was set constant initially. This induced an initial temperature gradient, which is different from most previous studies, where the initial temperature gradient implied an acceleration of the spontaneous wave velocity. A one-step chemistry facilitated preliminary computations. It is well known that the numerical results depend on the chemical kinetics model used[37,38]. However our conclusions and analysis of the flow characteristics, mainly qualitative, were expected to be very similar than those obtained considering a detailed chemical scheme.

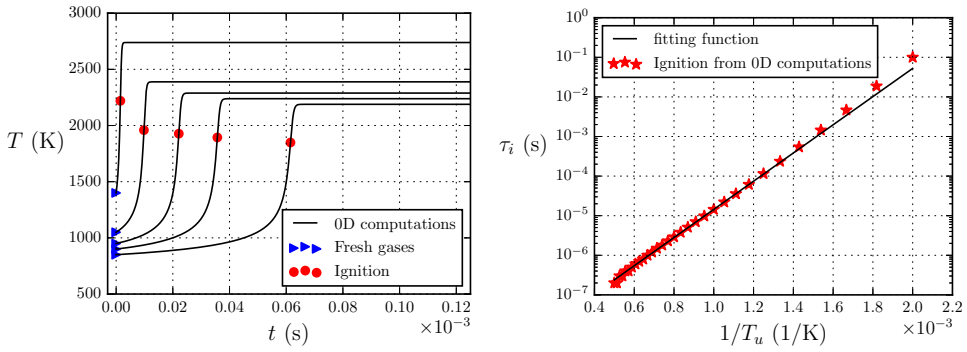

FIG. 1. Left: time evolution of the temperature (solid lines) for different values of fresh gas temperature T_u (green triangles) obtained from 0-D computations. Right : auto-ignition delay time (red circle) as a function of initial temperature T_u and the corresponding fitting function (solid line).

Following these assumptions, the initial conditions of the 2-D numerical setup consisted of two colliding subsonic diffusionless auto-ignition fronts propagating at constant speed and surrounded by inert hot layers. The reactive waves (RW) collided at a specified angle α, see Figure 3. The studied configurations were: 1-D and 2-D cases of a propagating constant-speed reactive wave, $\alpha = \pi$; 1-D case of a collision of plane reactive waves, $\alpha = 0$; 2-D case of an obtuse-angle collision, $\alpha = 2\pi/3$; 2-D case of an acute-angle collision, $\alpha = \pi/45$.

The reactive waves considered were the same for all cases. The angle of collision of the latter case and the thermodynamic state of fresh gases were chosen to facilitate computations and highlight the successive mechanisms of the detonation initiation.

Section II presents how the initial temperature profile was derived from the fact that the spontaneous reactive wave had initially a constant velocity. Section III describes the model and the problem statement. The numerical results are analyzed in Sect. IV for the different configurations listed above. Conclusions are drawn in Sect. V.

II. CONSTANT GRADIENT OF AUTO-IGNITION DELAY TIME

The computational domains were initially filled with burning gases. The corresponding fresh gases were representative of a stoichiometric hydrogen-air mixture at 16 atm. This initial pressure was chosen to be representative of the rapid compression machine available in our laboratory[39] or high-pressure burners[40]. Obtaining an auto-ignition wave with a constant velocity required a preliminary procedure, the objective of which was to carefully specify the initial conditions. From constant pressure 0-D reactor computations using the Cantera library with a global single-step reaction $\mathscr{R} \rightarrow \mathscr{P}$, the time evolution of density, temperature, and fresh gas mass fraction were determined for a large range of initial temperature T_u of the fresh gases, see Fig. 1 (left). Then, the ignition delay times were determined from the maximum temperature gradient, see red dot of Fig. 1 (left). The chemical reaction rate is an Arrhenius law: $\dot{\omega} = -kY_{\mathscr{R}} \exp(-E_a/RT)$. The reduced activation energy is $E_a/(RT_0)$=35 (T_0=300 K) and the pre-exponential factor $k = 2.6 \times 10^8\,\mathrm{s}^{-1}$ has been calibrated to obtain realistic ignition delay times comparable with those obtained using a detailed chemical mechanism in the high temperature range (1250 K-1500 K)[41]. The use of a detailed chemical scheme, the importance of which for being realistic is already well known[37], would complicate the physical interpretations of the mechanisms we are studying. It will also unreasonably increase the computation time. Thus, we decided to use the simplest chemistry, valid over a small range of fresh

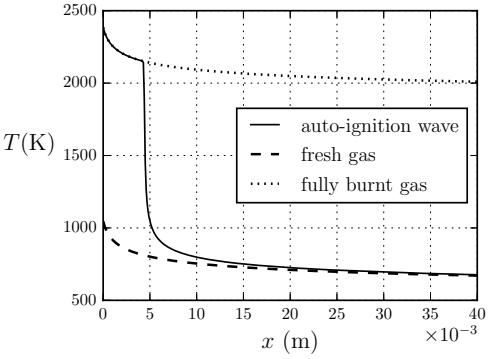

FIG. 2. Initial fresh gas temperature profile (dashed line), given by Eq. 4, leading to a constant speed auto-ignition wave. Corresponding fully burnt gas (dotted line). The solid line is an instantaneous profile at which instant the auto-ignition wave lies within the domain.

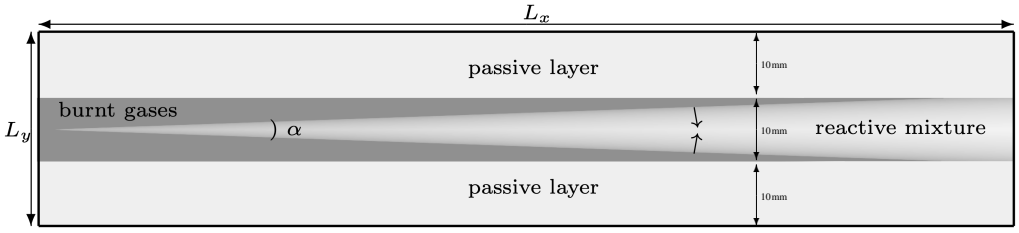

FIG. 3. Initial reactive front shape corresponding to a pair of plane auto-ignition waves colliding with the angle α and propagating towards the reactive mixture initially at constant speed.

gas temperature, in order to focus our analysis on the multidimensional collision mechanism, which we believe will remain similar in the detailed chemistry case. There will be however quantitative differences in the required initial conditions, the distance of transition and the (x,t) diagram for instance.

The ratio of specific heats and the heat release are $\gamma = 1.35$ and $q/RT_0 = 816.3$, respectively.
The ignition delay times τ can then be fitted (see Fig. 1-right) as a function of the initial temperature by:

$$\tau(T_u) = b\exp(a/T_u) \tag{1}$$

with $a = 8196.2\,\mathrm{K}$ and $b = 3.9830\times10^{-9}\,\mathrm{s}$, which is excellent in the range of 800 K-1400 K (temperature range corresponding to the initial conditions of the study leading to detonation initiation, see part IV D) and rather accurate in the range of 500 K-2000 K, see Fig. 1 (right). From Zeldovich [18], the spontaneous wave velocity can be deduced as:

$$S_n = (\mathrm{d}\tau/\mathrm{d}n)^{-1}, \tag{2}$$

integration of which yields the profile of the ignition delay time along the normal direction. For a constant velocity,

$$\tau(x_n) = (x_n - x_{mr})/S_n + \tau_{mr}. \tag{3}$$

The location of the first ignited point is thus x_{mr}, where the ignition time is the lowest and where the mixture is the most reactive. The inverse of Eq. (1), $T_u(\tau) = a/\log(\tau/b)$, combined with Eq. (3) gives the fresh gas temperature profile along the normal direction for which the auto-ignition front speed S_n is constant:

$$T_u(x_n) = a/\log\left[(x_n - x_{mr})/(S_n b) + \tau_{mr}/b\right]. \tag{4}$$

The dashed line of Figure 2 shows the fresh gas temperature profile for $\tau_{mr} = 10\,\mu\mathrm{s}$ and $S_n = 50\,\mathrm{m/s}$. Thus, a 10 µs delay is necessary before the beginning of the front propagation, velocity of which is 50 m/s. The solid line of Fig. 2 shows the temperature profile where the front has traveled about 5 mm during 100 µs. The dotted line corresponds to the fully burnt gases.

III. COMPUTATIONAL FRAMEWORK

A. Model and numerical methods

The flow is described by the multidimensional compressible reactive Euler equations with a single step chemistry for an ideal gas. An in-house code RESIDENT (REcycling mesh SImulations of DEtoNaTions) was used to solve the governing equations. Further description of the numerical methodology can be found in[42,43]. Briefly, a classical time-operator splitting method along with directional splitting is used to couple the hydrodynamics and chemistry. A HLLC Riemann solver is used to estimate the fluxes at the cell interfaces, after a high-order[44] interpolation procedure. A 3rd Runge-Kutta method is used for time integration. The parallelization of the code is achieved through a domain decomposition method (MPI). Typical computations were performed on 240 processors, with a cost of about 4800 CPU scalar hours. The total cost of the study is approximately one million hours.

B. Problem statement

Three computational domains were considered. The first was 1-D, $L_x = 240\,\mathrm{mm}$, with a cell size of $\Delta = 0.01\,\mathrm{mm}$. The second was also 1-D, $L_y = 30\,\mathrm{mm}$, with a cell size of $\Delta = 0.01\,\mathrm{mm}$. The third was 2-D Cartesian, $L_x \times L_y = 960\,\mathrm{mm}\times 30\,\mathrm{mm}$, with a cell size of $\Delta = 0.1\,\mathrm{mm}$. A convergence study has been conducted on the 2-D case where the grid cell size was decreased by a factor of two in both directions. The results showed that the deviation in the transition length, which was in our study about 480 mm, was less than 1.5%, see Appendix II.

The 2-D domain was initially filled with three distinct layers of gas, of which thickness being 10 mm in the y-direction for each layer, see Fig. 3. The thickness of the passive layer was set large enough so that it did not influence the phenomenon at play. Similar results were found when the thickness of the passive layers were doubled, see Appendix II. The two passive layers were inert gases at high temperature $\sim 500\,\mathrm{K}$ located on both sides of the reactive mixture. The central reactive layer initially contained an auto-ignition front separating burnt from fresh gases. Its shape corresponds to a

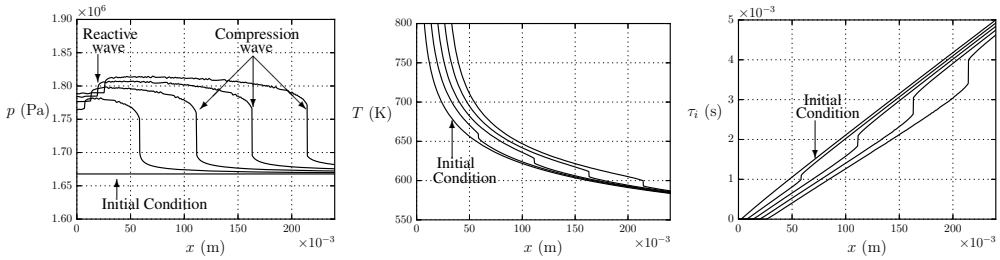

FIG. 4. Pressure (left) and temperature (middle) profiles at five different times with $\Delta t = 90\,\mu$s for a freely propagating auto-ignition wave (multimedia view). Right: profiles of remaining time before ignition at the same times.

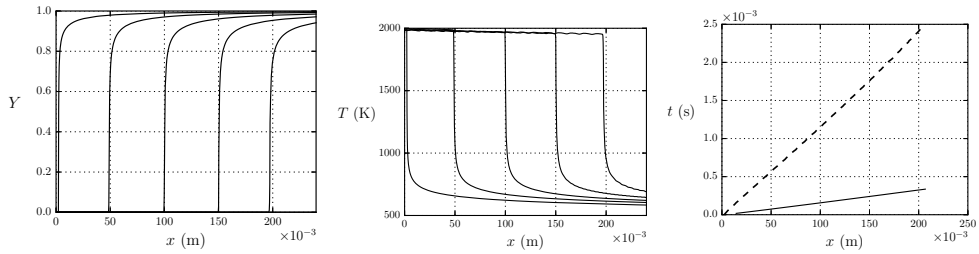

FIG. 5. Profiles of mass fraction of fresh gas Y_{fg} (left) and temperature (middle) at different instants of the simulations with $\Delta t = 500\,\mu$s for a freely propagating auto-ignition wave. Right: (x,t) diagram showing the compression wave (solid line) and reactive wave (dashed line) trajectories.

pair of plane auto-ignition waves colliding with the angle α. The reactive fronts are initially positioned such that their collision starts 10 mm from the left boundary and is centered in the y-direction. This configuration will be hereafter referred to as the V-shaped RW. All boundaries were wave transmissive.

The spatial distribution of the fresh gas variables was obtained from 1-D profiles (see solid line of Fig. 2). The density and mass fraction of fresh gas were then set as initial conditions in the normal direction of the reactive front surface whose position was initially imposed, see Fig. 3.

The complete fields used as initial conditions (density and mass fraction of fresh gas) for the whole set of cases studied (1-D and 2-D) are presented in Appendix I.

The two 1-D configurations corresponded to an horizontal line and a vertical line of the 2-D domain with respectively $\alpha = \pi$ and $\alpha = 0$. Accordingly, the two passive layers were only taken into account in the vertical line case. Two different temperatures of the passive layers (~ 500 K and ~ 200 K) were considered in this latter case to study the acoustic impedance effect of these layers.

IV. NUMERICAL RESULTS AND ANALYSIS

A. Propagating reactive wave - $\alpha = \pi$

First, the propagation of a plane front is analysed setting $\alpha = \pi$, see Fig. 3. The problem reduced to a 1-D case in the x-direction if the influence of the inert layers are neglected. The profiles of pressure and temperature for several instants of the simulation are presented in Fig. 4 (left and middle). The temperature scale focused on the fresh gas conditions and the time intervals have been chosen to highlight the appearance of a compression wave during the initial transient whose speed is large in comparison with the RW speed. This compression wave set the gas into motion[45], consistently with the reactive wave speed. Its effect on temperature is small although the chemical rate may increase significantly. Accordingly, the remaining time before ignition τ_i is also shown in Fig. 4-right. In its theoretical work, Kassoy[45] indicated how the hot spot expansion can be *the source of fluid expelled from the original finite volume and is a 'piston-effect' source of acoustic mechanical disturbances beyond the spot.* In this case, the hot spot was finite and was bounded by a wall. In order to decrease these influences, both the absence of walls (responsible for enhanced thermal feedback[5]) and the use of constant gradient of the ignition delays (instead of constant gradient of

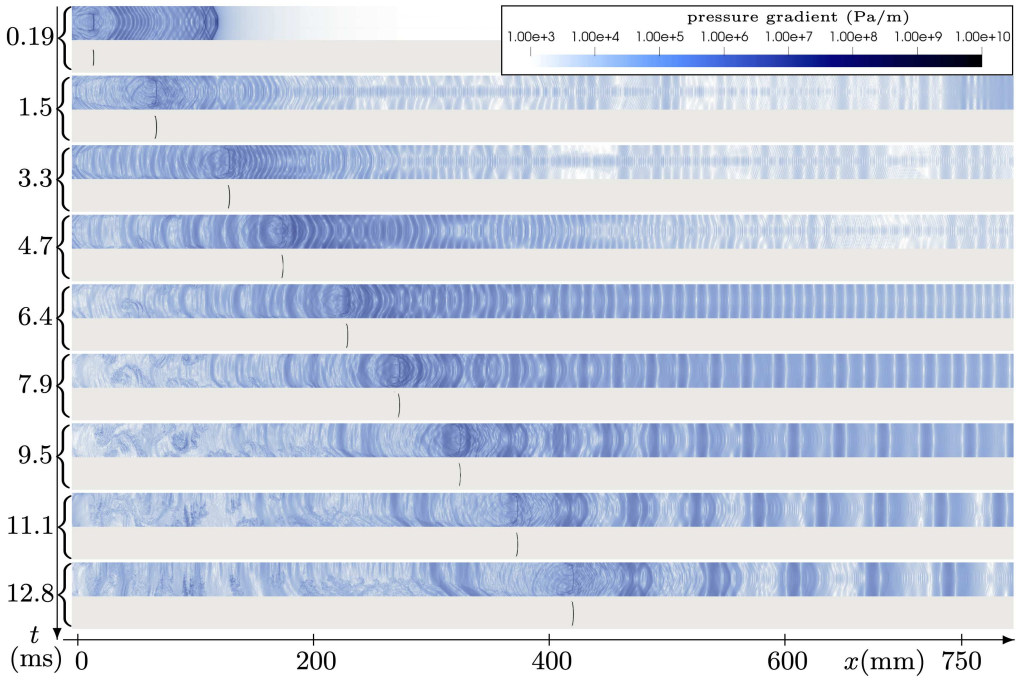

FIG. 6. 2-D results at nine time steps of the propagation of the reactive wave. The pressure gradient fields are coloured in blue and the grey frames show the corresponding isoline of chemical rate $\dot{\omega}_{max}/2$, depicting the reactive wave shape and position (multimedia view).

temperature, as usually done in literature) were found in our computations to decrease the amplitude of this initial compression wave.

The initial profile of remaining time before ignition is a straight line as given by Eq. 3. As expected, the temperature small jump could be associated with a fall in the induction time (see Fig. 4-right). Figure 5 (left and middle) shows the evolution of the fresh gas mass fraction Y_{fg} and the temperature using the full scale range where the time intervals have been chosen to put into evidence the reactive wave propagation. The initial condition corresponds to the most left curve. Figure 5-right shows the trajectories of the weak compression wave and the reactive wave. The former propagates at about the sound speed and the latter is largely subsonic but both propagate at nearly constant velocities.
In this sharp gradient case, according to Kapila *et al.*[19]'s terminology, the initial transient of the energy release induced a weak compression wave. After this small decrease of the ignition time, the profile of τ_i remained linear. This meant that the reactive wave velocity was still constant after the leading shock wave passage, and that the latter was rather weak. This was confirmed from Fig. 5. The value of the slope of the induction time profile could not correspond to what was imposed initially, i.e. 50 m/s but was larger, i.e 70 m/s due to the thermal feedback of the leading shock wave. The (x,t) diagram in Fig. 5-right displays the divergence between the reactive wave (dashed line) and the leading shock wave (solid line) whose velocity was about 600 m/s. This value varied slightly due to the temperature variation in fresh gases. The reaction zone and the leading shock were then not coupled in this 1-D case, both velocities being an order of magnitude different. The pressure wave was not amplified and a reactive wave of constant speed propagated. Consequently, without any more acceleration and no more compression waves, no transition to detonation occurred.

In order to analyse the effects of the inert layers, a 2-D simulation of the propagation of the reactive front has also been performed. Figure 6 presents, as a (x,t) diagram, the pressure gradient fields (blue) and corresponding reactive wave (grey: isoline of chemical rate $\dot{\omega}_{\max}/2$) at nine time steps. Here again, the divergence between the reactive wave and the leading shock wave was observed. The latter was only visible at the first time step at 0.19 ms and was out of the domain for the other time steps. This 2-D simulation also highlighted that the RW topology cannot be considered anymore as 1-D.

First, the interaction of the reactive front with the inert layers was found to be another emission source of acoustic

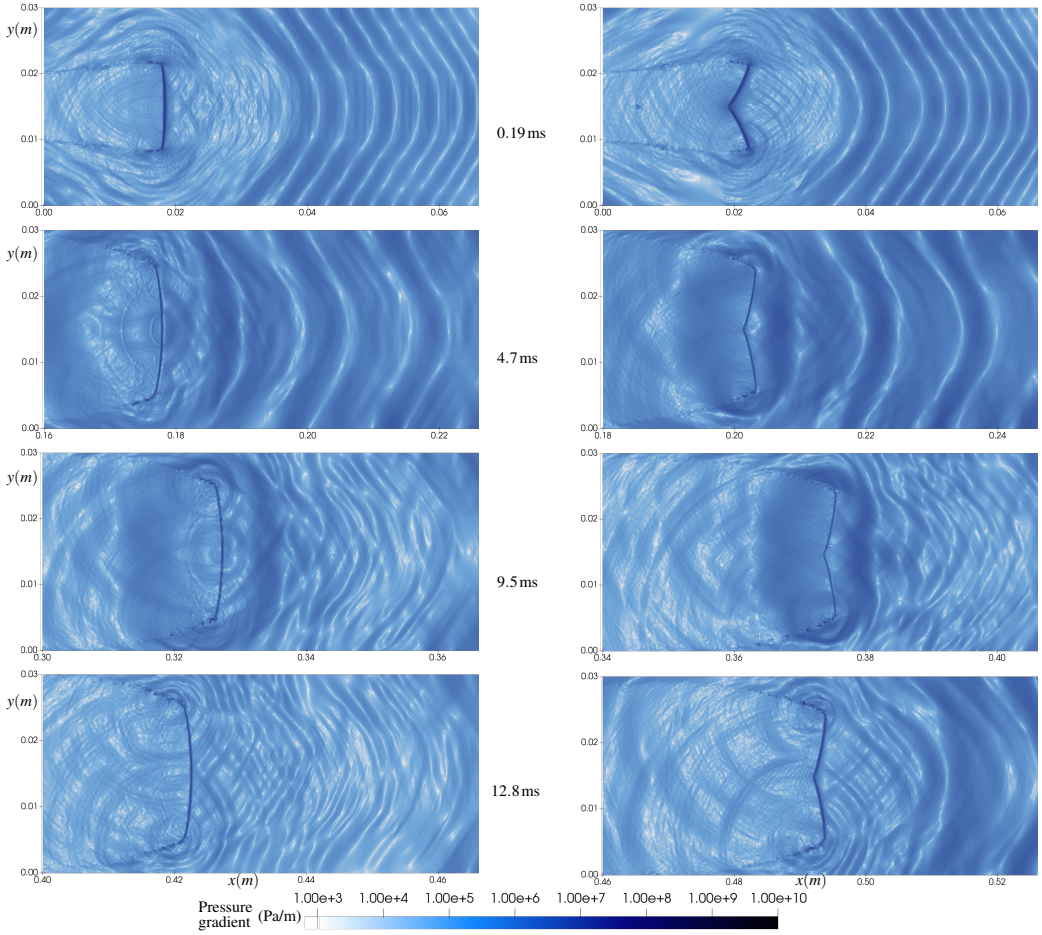

FIG. 7. Zoom of four images of Figs. 6 and 11: fields of 2-D pressure gradient at four time steps of the propagation of the reactive wave. Left: $\alpha = \pi$. Right: collision of auto-ignition fronts with an obtuse-angle $\alpha = 2\pi/3$.

waves, see Figure 7-left where four times from Figure 6 were zoomed. Indeed, a barocline effect was present due to the misalignment of the pressure wave gradient due to the reactive front shape and the density gradient due to the inert hot layer. A vortex point source was thus present at the intersection of the reactive wave with the inert layer, source of pressure waves.

The amplitude of these compression waves and induced temperature increase were not sufficient enough to increase the reaction rate significantly. This was consistent with the low-Mach speed of the reactive front imposed initially. Accordingly, no front acceleration was observed, see Figure 6. The same conclusion can be drawn from the analysis of the temperature fields and isolines of remaining times before ignition presented in Figure 8-left. The initial pressure wave modified certainly the fresh gas conditions but the reactive front speed remained constant afterwards. Thus, in this 2-D case, the pressure waves induced by the reactive wave and inert layer interaction were too weak to enable any transition.

The second important consequence of the presence of inert layers was the transverse gas expansion of burnt gases, which is clearly visible in Fig. 8-left. This mechanism is correlated with the increase in temperature and decrease of density through the reaction zone. The flow being subsonic, this expansion also took place in the fresh gases upstream of

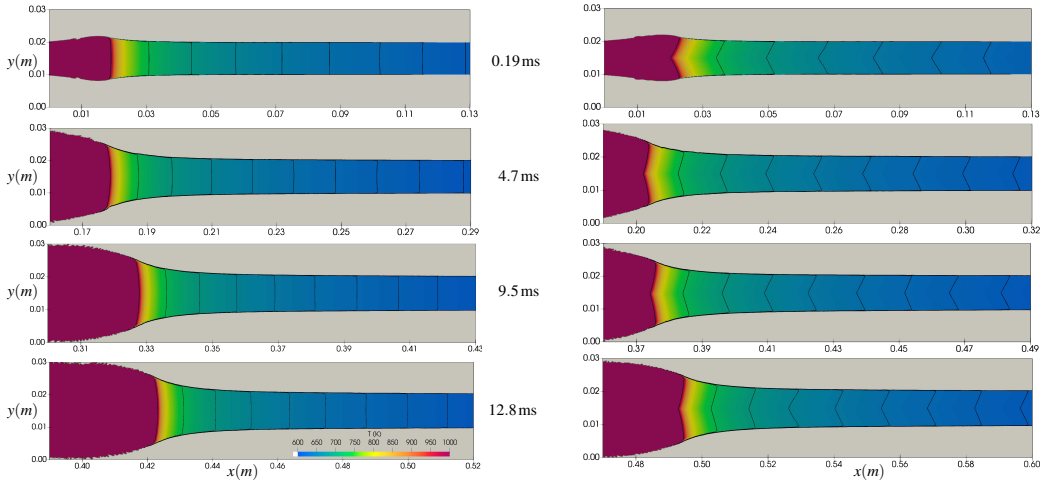

FIG. 8. 2-D temperature fields at four time steps of the propagation of the reactive wave. Left: $\alpha = \pi$. Right: collision of auto-ignition fronts with an obtuse-angle $\alpha = 2\pi/3$, associated with isovalues of remaining times before ignition taken with 300 µs step.

the reactive wave. The related flow divergence stretched the flow in the y-direction and therefore strengthened the temperature gradients in the x-direction. Accordingly, the propagation speed of the auto-ignition front decreased to reach a value near 30 m/s, below the initial 50 m/s. Therefore, in this 2-D case, the reactive-hydrodynamic wave speed first increased due to the leading shock thermal feedback, similarly to the 1-D case, but then decreased due to the flow divergence allowed by the presence of inert layers. Stretching also slightly distorted the RW, which became convex.

Eventually, the numerical results obtained in the limit case of subsonic auto-ignition fronts with $\alpha = \pi$ demonstrated that the carefully designed initial condition along with open boundaries made it possible to obtain a RW wave of constant speed.

B. 1-D collision of plane reactive waves - $\alpha = 0$

Another limit case corresponds to the plane collision of subsonic auto-ignition fronts, with $\alpha = 0$. A gap of 8 mm between the opposite reactive fronts was set initially. Here, the problem simplified to 1-D in the y-direction.

Figure 9 displays profiles of pressure, temperature and mass fraction of fresh gases for two different temperatures of the inert layers. The first instant is the initial condition and the other instants were chosen to follow the reactive wave displacement and the evolution of their structure, which is maintained during the simulation until the collision. They intersected with each other at the center of the domain, the problem being symmetric (see Figure 9). The propagation speed was slightly higher with cold inert layers due to the stronger influence of the reflected compression waves: the acoustic impedance of the passive layers induced a second thermal feedback. Accordingly, the rise in pressure was greater and the reactive layer widened further for low temperature of the passive layers.

Figure 10 displays the profiles of pressure, temperature and remaining time before ignition at different instants for these two 1-D cases. The profiles of remaining time before ignition were almost straight lines (see Figure 10-right). The graph scales and the time step between each profile were chosen to follow the leading compression wave displacement generated by the initial transient.

At the first instant presented in Figure 10, respectively the coldest temperature profile and the largest delay time profile, the compression waves as well as their further back and forth evolution were mainly visible in the pressure profiles. Then, at the second instant, the leading waves propagated towards fresh gases, see arrow 1 in Fig. 10. These waves collided at the domain center, see arrow 2, and then traveled back into the reactive zone, see arrow 3. This initial transient had also produced two compression waves propagating towards the burnt gas side, which are partly reflected by the inert gas layers. These two waves traveled back to the fresh gas side but with a smaller amplitude, see arrow 4. The amplitude of this secondary wave depended on the acoustic impedance mismatch of the inert and reactive layers[46,47]. Accordingly, this amplitude was higher with cold inert layers so the fresh gases were submitted to a larger increase of temperature and decrease of remaining time before ignition. This result explains the larger RW propagation speed obtained with cold inert layers. Eventually, four compression waves (two back and forth) induced by these initial transients passed through the fresh gases, mod-

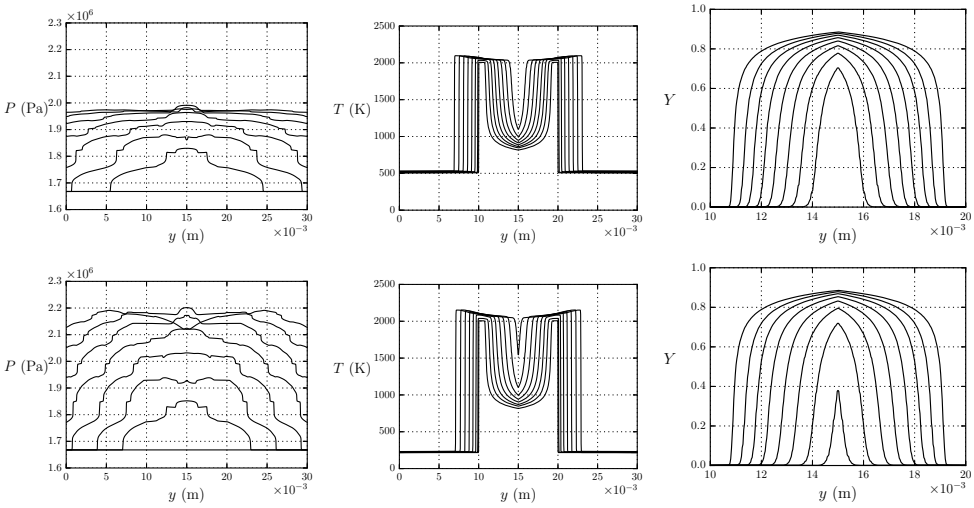

FIG. 9. Profiles of pressure (left), temperature (middle), and mass fraction of fresh gas (right) at different times with $\Delta t = 9\,\mu$s for a front plane collision of two auto-ignition waves with inert layers at $\sim 500\,$K top (multimedia view) and $\sim 200\,$K (bottom).

ifying subsequently the induction time that however remained almost linear, see Fig. 10-right. Therefore, similarly to the propagating case, the velocity of the colliding reactive waves were still constant after the compression wave passages. The velocity of the RW, initially defined to be $50\,$m/s, increased to $80\,$m/s after the thermal feedback occurred. Therefore, the front propagation speed remained largely subsonic so the transition to detonation did not occur in this case neither. The velocity of the RW could be expected to be enhanced in confined flow with walls instead of the inert interfaces. In this case, the amplification of the velocity would have beared some similarities to the double thermal feedback discussed in Clavin and Tofaili[5].

C. Obtuse-angle 2-D collision of reactive waves - $\alpha = 2\pi/3$

The collision of two plane auto-ignition fronts with $\alpha = 2\pi/3$ is now considered. Figure 11 presents the pressure gradient fields (blue) and corresponding RW (grey : isoline of chemical rate $\dot{\omega}_{\max}/2$) at the same nine time steps and with the same colour scales than those for $\alpha = \pi$ presented in Fig. 6. Four different times of this figure are zoomed and presented in Fig. 7-right. The temperature fields and isolines of remaining time before ignition are presented in Fig. 8-right.

Similar conclusions than those with $\alpha = \pi$ were drawn and are recalled here.
The initial transient induced shock has been evacuated from the domain. This induced a slight increase of the RW velocity.
The pressure waves, which were generated at the intersection of the RW and the passive layers were too weak to modify significantly the fresh gas conditions. As a consequence, there was no more RW acceleration.
The gas expansion induced flow divergence that stretched the flow in the y-direction, which increased the temperature gradient. This resulted in the decrease of the RW velocity.

In this case, stretching also increased the value of the collision angle so that the reactive front became almost flat. It should be emphasised that with the very specific initial condition used and if the hydrodynamics had been neglected, the shape of the reactive front and therefore the collision-angle would have been preserved during the propagation. The propagation speed in the x-direction of the global RW structure was slightly higher with $\alpha = 2\pi/3$ than with $\alpha = \pi$ but remained largely subsonic. The slightly higher value of RW area with $\alpha = 2\pi/3$ than with $\alpha = \pi$ was not sufficient for detonation transition to occur.

D. Acute-angle 2-D collision of reactive waves - $\alpha = \pi/45$

The collision of two plane auto-ignition fronts with a very small angle $\alpha = \pi/45$, with the same reactive front structure as in previous subsections has been performed.

Figure 13 presents the pressure gradient fields (blue) and corresponding RW (grey: isoline of chemical rate $\dot{\omega}_{\max}/2$) with the same colour scales than in Fig. 6 and 11. The collision induced a very rapid motion of the RW tip in the x-direction. The induced pressure waves, unlike the previous cases $\alpha = \pi$ and $\alpha = 2\pi/3$, were not faster in the x-direction than the V-shaped RW. Their amplitude ahead in the fresh

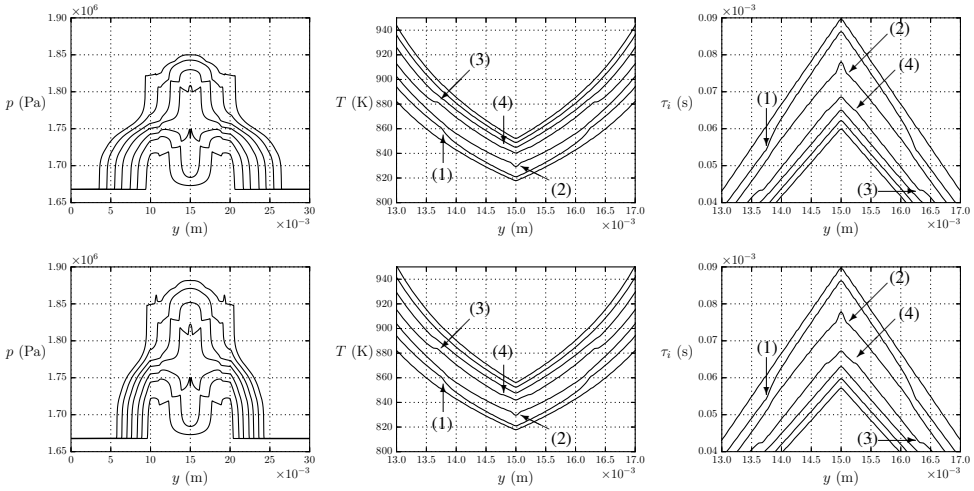

FIG. 10. Profiles of pressure (left) and temperature (middle) at six different times with $\Delta t = 1.9\,\mu$s for a front plane collision of two auto-ignition waves. Right: profiles of remaining time before ignition. Top: hot inert layers $\sim 500\,$K (multimedia view). Bottom: cold inert layers $\sim 200\,$K.

gases was also stronger. The V-shaped RW accelerated until coupling with the pressure waves and transition to detonation, before $370\,\mu$s.

During the first instants ($0 < t < 267\,\mu$s), the RW shape was maintained but became more compact with a decrease of the RW surface. Then, the RW shape changed ($267\,\mu\text{s} < t < 316\,\mu$s) until the almost flat detonation front was obtained ($t > 316\,\mu$s).

Figure 12 shows eight temperature fields at different times and isolines of remaining times before ignition (left) and pressure gradients near the reaction zone position. Similarly to the previous case $\alpha = 2\pi/3$, during the first instants, the collision angle increased. However, the gas expansion widening the central layer occurred only in the fully burnt gases in this case, see Figure 12. Accordingly, the stretching can not solely be responsible for the RW surface reduction.

The topology of the V-shaped RW consisted initially of straight lines and its velocity in the x-direction can be estimated from Eq. 5.

$$S_x = \frac{S_n}{\sin(\alpha/2)}. \tag{5}$$

According to the initial condition set for the RW wave speed, i.e. $50\,$m/s and Eq. 5, the speed of the V-shaped RW is initially $1430\,$m/s. Similarly to the other cases ($\alpha = \pi$ and $\alpha = 2\pi/3$), the RW propagation speed in the normal direction slightly increased so the V-shaped RW speed also slightly increased to reach a maximum which is supersonic: $S_x \simeq 1900\,$m/s after the transients, see the solid line of Figure 15.

As in the obtuse case, the interaction of the RW (arrow 1 in Fig. 12) with the hot passive layers was a source of vorticity due to barocline effect and of pressure waves. Thus, oblique Mach lines appeared in this case (arrow 2 in Fig. 12), reflecting upon the RW surfaces. In the second and third frames of Figure 12 (corresponding to $181\,\mu$s, $267\,\mu$s), the lines of the V-shaped RW were no longer straight after interaction with amplified compression waves. Thus, a change in curvature was observed, which got gradually amplified as seen in the fourth frame at $305\,\mu$s. As a result of the back and forth pressure waves, the Mach lines focused and got amplified to form a train of oblique shock waves. Thus downstream of these compression waves, inside the V-shaped RW, the velocity of fresh gases decreased. Moreover, in such exothermic supersonic flows, the trajectories of burnt gas tend to realign with the pressure waves[48,49]. These features were responsible for the reduction of the RW area.

This phase on the fourth frame was also accompanied with a thicker reaction zone that reduced in the next steps.

The RW fronts acted as surfaces of reflection for the oblique shocks, forming a self-resonating system. Two zones then emerged in the center of the domain (arrow 3 in Fig. 12) where wave focusing and subsequent heating were more prominent than near the edges. One "wave focusing zone" (WFZ) was located in the fresh gases and the other one was near the tip. The RW fronts got further deformed due to the successive impact of shocks along their surface, with a great change in the curvature. The first zone then gave rise to a suddenly accelerating RW (arrow 4 in Fig. 12) that was amplified by strengthened shock waves until the formation of an overdriven detonation (see at $312\,\mu$s and $315\,\mu$s). A pocket of fresh gases got encap-

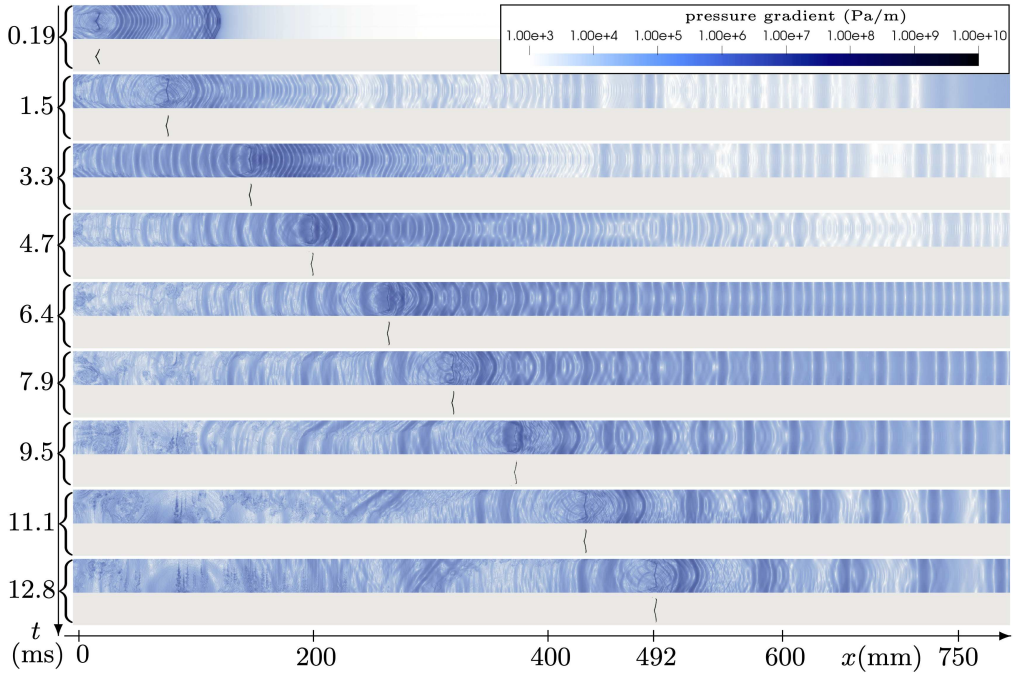

FIG. 11. 2-D results at nine time steps of the obtuse-angle ($\alpha = 2\pi/3$) collision of reactive waves. The pressure gradient fields are coloured in blue and the grey frames show the corresponding isolines of chemical rate $\dot{\omega}_{\max}/2$, representing the reactive front shape and position (multimedia view).

sulated, whose further combustion along with the presence of the second WFZ generated a retonation (at $305\,\mu s < t < 323\,\mu s$ of Fig. 12) moving backwards towards the burnt gases.

Finally, a detonation wave propagated with oblique shocks present in the hot inert layers. Some vortical structures were also present at the interface between the burnt and the inert gases, due to the barocline effect. These structures are visible on the density gradient field presented in figure 17.

The x-positions of the reactive waves, determined when $Y_{fg} \simeq 1‰$, and of the leading compression waves[19] taken at the domain center are shown in Fig. 14-left. The (x,t) diagram obtained for the acute angle case is compared to the previous obtuse angle case (Fig. 14-right).
In the first zone (I), the two waves diverged rapidly, as the compression waves emitted by the initial transients were faster than the reactive wave. The same features were obtained in the obtuse angle case (Fig. 14-right). In the second quasi-stable transients (II), the compressive wave path represents the trace of the oblique shocks at the center of the channel. The reactive wave path represents that of the tip of the V-shaped RW. The apex then catched up with the continuously generated oblique shocks. During the transition (III) between 400 mm and 500 mm, the RW tip abruply accelerated. The two waves relaxed to the same value and were coupled in zone (IV). This result was consistent with the onset of the cellular structure observed in the numerical soot foil presented in Figure 17-top, marker of the gaseous detonation. This observation attests to the coupling between the two waves and thus to the presence of a detonation.

Figure 15 shows the evolution of the speeds of the compressive wave and the RW after the initial transient for all the cases investigated. The global initial evolution of the acute case followed that of no-go cases, before a rather abrupt acceleration to an overdriven detonation, before relaxation towards a stable detonation.

The combustion mode before detonation can be further analyzed with the (v,p) and (Y,p) diagrams[19] taken on the center of the channel (see Fig. 16). At the very beginning of the propagation phenomenon (at 87 µs, zone (I) of the (x,t) diagram of Fig. 14-left), a pressure increase was observed on the fresh gas side of the reaction zone (determined from $1 - Y_{fg} \simeq 0.1\%$) followed by a gradual decrease in pressure. The compressive part can be seen as a weak detonation whereas the relaxation part is similar to what one would observe inside the structure of a subsonic deflagration. Then a train of shocks emerged at the beginning of the weak deflagration (at 240 µs).

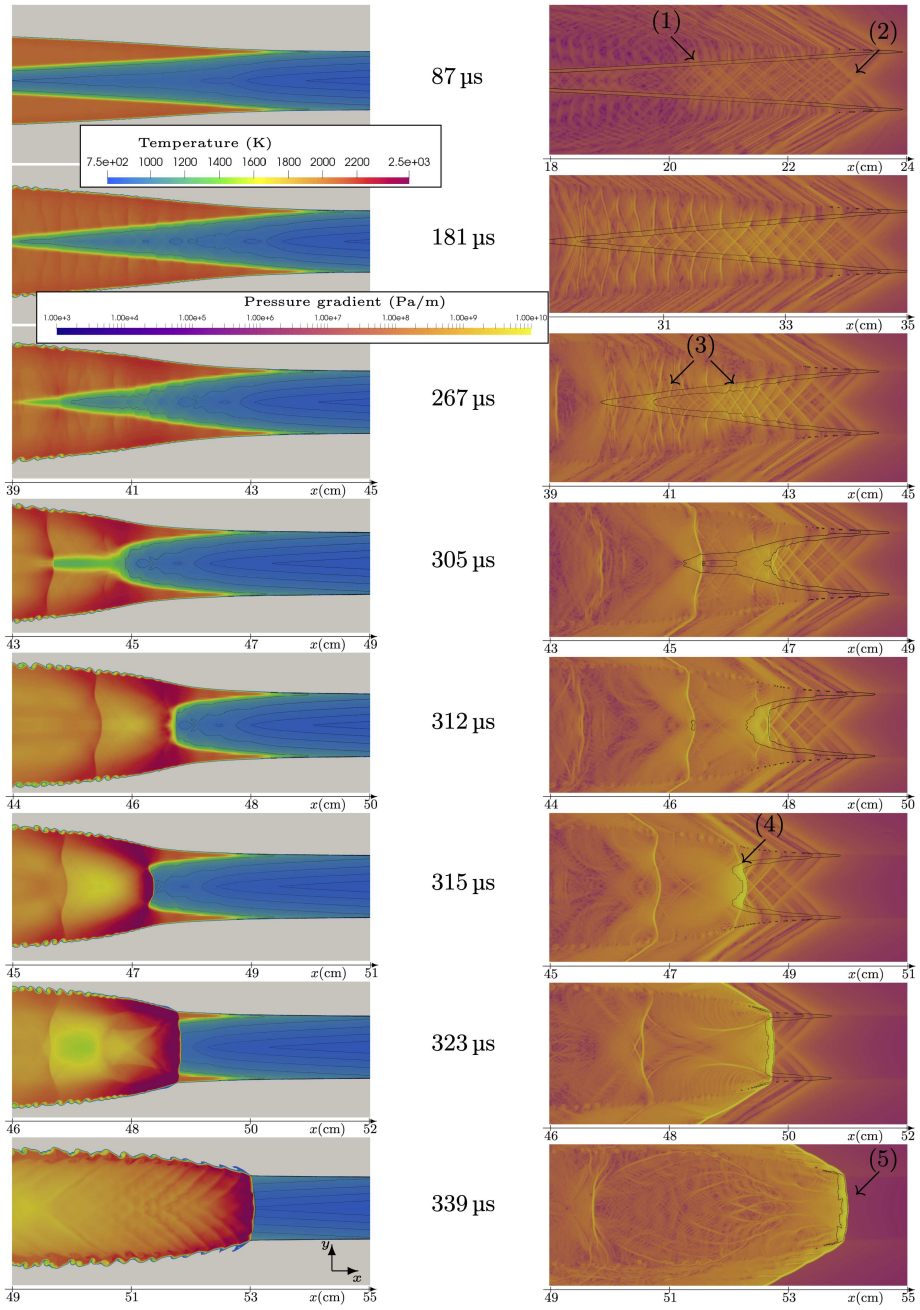

FIG. 12. 2-D temperature fields associated with isovalues of remaining times before ignition taken with 25 µs step (left) and 2-D pressure gradient fields (right) at eight time steps of the acute-angle ($\alpha = \pi/45$) collision of reactive waves (multimedia view).

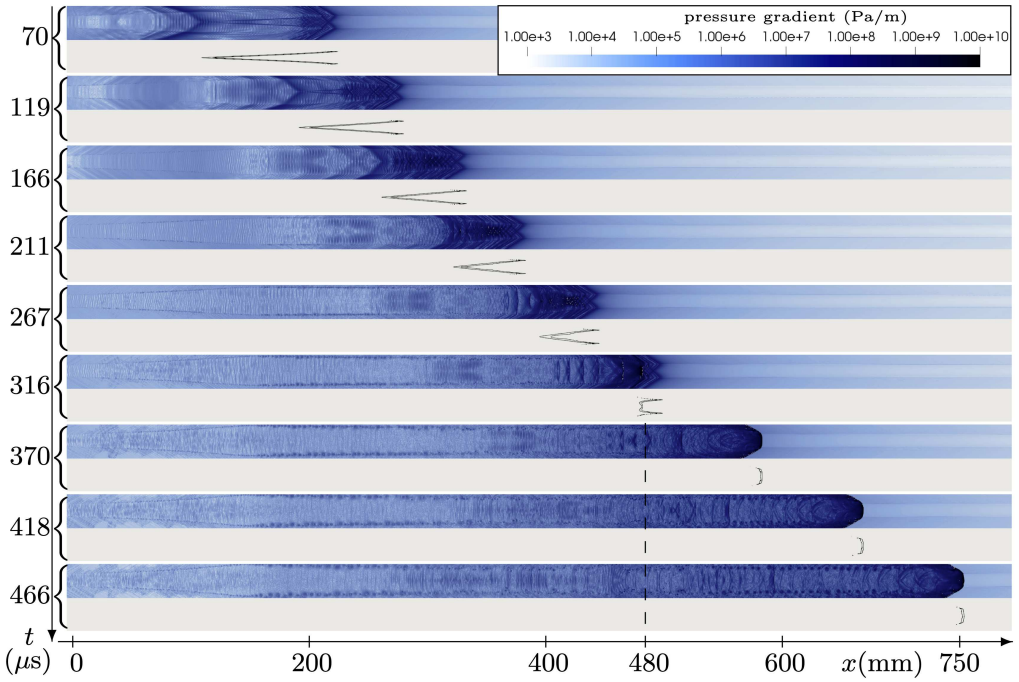

FIG. 13. 2-D results at nine time steps of the acute-angle ($\alpha = \pi/45$) collision of reactive waves. The pressure gradient fields are coloured in blue and the grey frames show the corresponding isolines of chemical rate $\dot{\omega}_{\max}/2$, representing the RW shape and position (multimedia view).

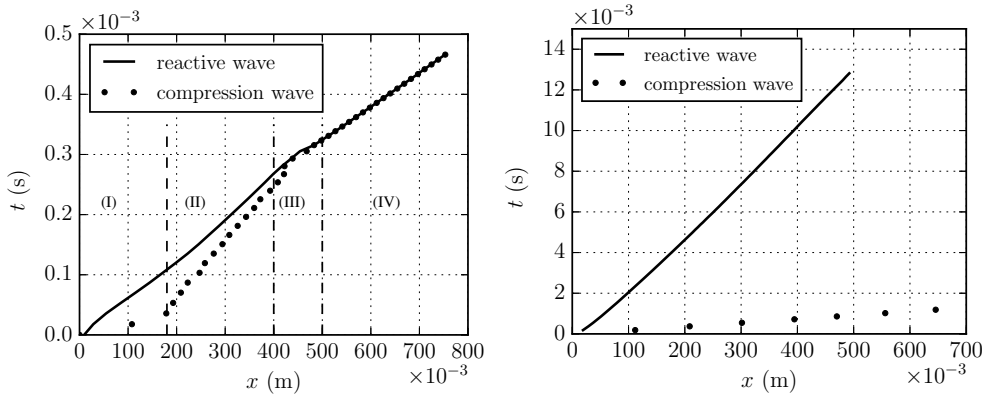

FIG. 14. (x,t) diagrams of the reactive wave and leading compression wave at the domain center along the x-direction for the acute-angle ($\alpha = \pi/45$) case (left) and the obtuse-angle ($\alpha = 2\pi/3$) case (right). (I) initial transient, (II) quasi-stable leading shock waves, (III) transition to detonation and (IV) quasi-stable detonation.

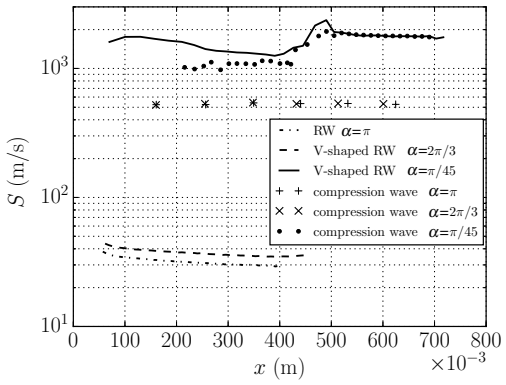

FIG. 15. Wave propagation speeds for the plane ($\alpha = 2\pi/3$), the obtuse-angle ($\alpha = 2\pi/3$) and the acute-angle ($\alpha = \pi/45$) cases.

They represent the trace of the oblique shocks on the center of the domain. They appeared as a source of pressure fluctuations during the deflagration-type pressure decay. Then they merged into stronger shocks (at 305 µs), corresponding to the two WFZ, identified in Fig. 12. The slopes of the deflagration part have greatly increased. Eventually, these two shocks merged before transition to detonation.

Figure 17-top shows the numerical soot foil determined from the pressure maxima. The location of the transition to detonation can be easily determined. Figure 17-bottom shows the 2-D Schlieren field for the last instants of the simulation. The window included the pattern left by the occurrence of the transition on the left part of the window. The physical mechanisms involved during the transition have left a specific pattern, which showed the successive expansions and contractions that the reactive layer has undergone at these instants. This specific pattern bears some similarities with the post-mortem features obtained in the another context of DDT in loosened porous explosive (Fig. 5 in Parker *et al.* [50]).
On the right side, the triple points can be seen, coming mainly near the center of the channel. The vortical structures between the burnt gas and inert layers produced by barocline mechanism also appear clearly.

V. DISCUSSIONS AND CONCLUSIONS

A simple 2-D configuration showed that the folding of fast reactive fronts, driven by reactivity gradients is a powerful mechanism that can very efficiently initiate a detonation, on the contrary of its 1-D counterpart. The topology of the reactive waves consisted of two subsonic colliding auto-ignition fronts, bounded by hot inert layers. The angle between the collisions was rather low. The interaction of the reactive phase wave, propagating subsequently at a supersonic speed, constituted a continuous source of vorticity. The latter induced oblique pressure waves, of which self-resonance near the center of the channel in the fresh gases accelerated the RW fronts until transition to detonation. Our study showed that the spontaneous wave can evolve from an initial subsonic to the CJ velocity, most likely in the restricted area of the funnel of unreacted material, previously shaped by the flow, seen in some DDT scenarios near the tip of a turbulent flame zone whether in experiments[1] or in computations[51,52]. The analysis of Chambers *et al.* [30] showed that a compressed region was formed ahead of non-planar flames, on the verge to collide, after which the runaway flame occured. A careful analysis of the temporally and spatially resolved experimental results of Meyer, Urtiew, and Oppenheim [1] showed that oblique shocks were also present within the tongue of fresh gases, see frames 3 to 7, as well as the occurrence of two explosion events. The numerical results of the present study, even if they were obtained under different conditions, seem to be in good qualitative consistency to certain observations of these latter experiments. Therefore, it seemed reasonable to conclude that the scenario described in this numerical experiment could also be obtained with more realistic conditions.

The present study unraveled the influence of the geometry of the reactivity gradients, as it provides the seeds for the coupling between gasdynamics and heat release. The collision of two subsonic auto-ignition fronts with initial constant velocity was found to transit to detonation only when the collision angle was acute. Continuous pressure fluctuations and oblique shocks coming from vorticity sources and sheets from barocline effects can subsequently enhance this transition. The transition length would even be shorter if a wall confinement have been considered. This path to transition can be complementary to that which invokes mixing burning within non-planar turbulent flame brush. Now that the role of the collision angle is clearly identified and the canonical numerical experiment is described, many studies can be carried out, such as studying the influence of chemistry at low temperature, identifying the critical angle triggering transition and studying the effects of the acoustic impedance of boundaries.

VI. ACKNOWLEDGEMENTS

The computations were performed using HPC resources from GENCI-CINES (Grant A0132B07735). This work was supported by the CPER FEDER Project of Région Nouvelle Aquitaine. This work pertains to the French Government program "Investissements d'Avenir" (EUR INTREE, reference ANR-18-EURE-0010)

APPENDIX I : INITIAL CONDITION FIELDS

This appendix describes the initial conditions used for each simulation case considered in this study in terms of density fields and mass fraction fields of fresh reacting gas. The gas is initially motionless and the pressure is constant, see sections II and III for more details.

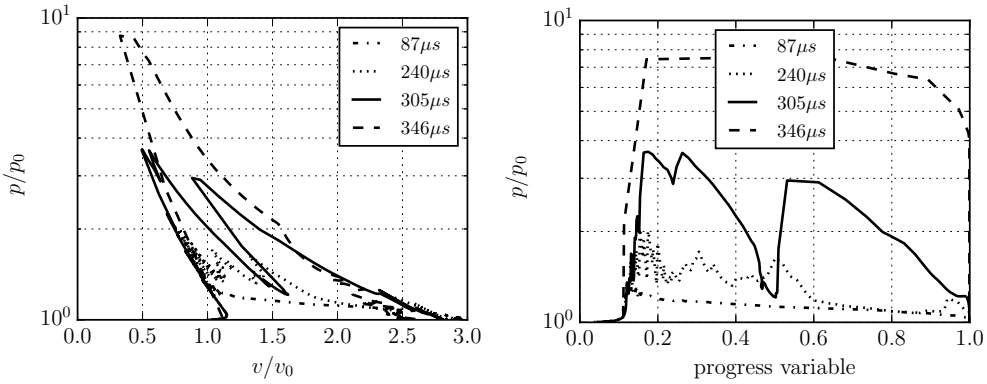

FIG. 16. Left: Pressure-specific volume diagram ($p_0 = 16$ atm, $v_0 = 6.2\,\mathrm{m}^3/\mathrm{kg}$). Right: Pressure-progress variable diagram.

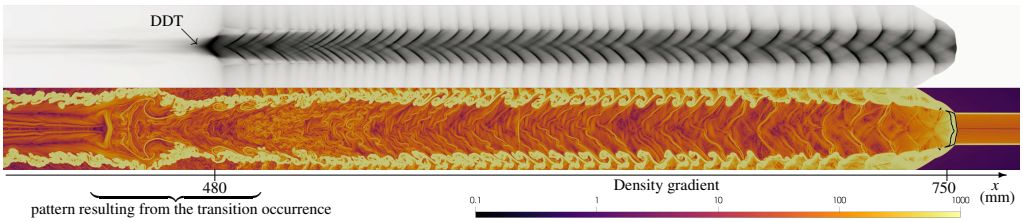

FIG. 17. 2-D Numerical soot foil (top) and density gradient field (bottom) at 466 µs of the acute-angle ($\alpha = \pi/45$) case (multimedia view).

See Figures 18 and 19 for 1-D domain and Figures 20 to 25 for 2-D domain.

APPENDIX II : CONVERGENCE STUDIES

See Figures 26 for the mesh sensitivity analysis and and 27 for the study of the distance of boundaries.

APPENDIX III

Full numerical results can be downloaded upon request to the corresponding author

[1] J. Meyer, P. Urtiew, and A. Oppenheim, "On the inadequacy of gasdynamic processes for triggering the transition to detonation," Combust. Flame **14**, 13–20 (1970).
[2] H. Yang and M. I. Radulescu, "Enhanced DDT mechanism from shock-flame interactions in thin channels," Proc. Combust. Inst. **38**, 3481–3495 (2021).
[3] Y. Ballossier, F. Virot, and J. Melguizo-Gavilanes, "Strange wave formation and detonation onset in narrow channels," J. Loss Prevent. Process Indust. **72**, 104535 (2021).
[4] C. A. Towery, A. Y. Poludnenko, and P. E. Hamlington, "Detonation initiation by compressible turbulence thermodynamic fluctuations," Combust. Flame **213**, 172–183 (2020).
[5] P. Clavin and H. Tofaili, "A one-dimensional model for deflagration to detonation transition on the tip of elongated flames in tubes," Combust. Flame **232**, 111522 (2021).
[6] E. S. Oran and V. N. Gamezo, "Origins of the deflagration-to-detonation transition in gas-phase combustion," Combust. Flame **148**, 4–47 (2007).
[7] J. H. Lee, *The detonation phenomenon* (Cambridge University Press, 2008).
[8] P. Clavin and G. Searby, *Combustion waves and fronts in flows: flames, shocks, detonations, ablation fronts and explosion of stars* (Cambridge University Press, 2016).
[9] A. Khokhlov, E. S. Oran, and J. C. Wheeler, "Deflagration-to-detonation transition in thermonuclear supernovae," Astrophys. J. **478**, 678 (1997).
[10] D. Schwer and K. Kailasanath, "Numerical investigation of the physics of rotating-detonation-engines," Proc. Combust. Inst. **33**, 2195–2202 (2011).
[11] V. Anand and E. Gutmark, "Rotating detonation combustors and their similarities to rocket instabilities," Prog. Energy Combust. Sci. **73**, 182–234 (2019).
[12] Y. Wang, J. Liang, R. Deiterding, X. Cai, and L. Zhang, "A numerical study of the rapid deflagration-to-detonation transition," Physics of Fluids **34**, 117124 (2022).
[13] A. Robert, S. Richard, O. Colin, and T. Poinsot, "LES study of deflagration to detonation mechanisms in a downsized spark ignition engine," Combust. Flame **162**, 2788–2807 (2015).
[14] Z. Wang, H. Liu, and R. D. Reitz, "Knocking combustion in spark-ignition engines," Progress in Energy and Combustion Science **61**, 78–112 (2017).
[15] Q.-h. Luo and B.-g. Sun, "Inducing factors and frequency of combustion knock in hydrogen internal combustion engines," international journal of hydrogen energy **41**, 16296–16305 (2016).
[16] Y. Li, W. Gao, P. Zhang, Z. Fu, and X. Cao, "Influence of the equivalence ratio on the knock and performance of a hydrogen direct injection internal combustion engine under different compression ratios," International Jour-

nal of Hydrogen Energy **46**, 11982–11993 (2021).
[17]A. Y. Poludnenko, J. Chambers, K. Ahmed, V. N. Gamezo, and B. D. Taylor, "A unified mechanism for unconfined deflagration-to-detonation transition in terrestrial chemical systems and type ia supernovae," Sci. **366** (2019), https://doi.org/10.1126/science.aau7365.
[18]Y. Zeldovich, "Regime classification of an exothermic reaction with nonuniform initial conditions," Combust. Flame **39**, 211–214 (1980).
[19]A. Kapila, D. Schwendeman, J. Quirk, and T. Hawa, "Mechanisms of detonation formation due to a temperature gradient," Combust. Theory Model. **6**, 553 (2002).
[20]M. Kuznetsov, M. Liberman, and I. Matsukov, "Experimental study of the preheat zone formation and deflagration to detonation transition," Combust. Sci. Technol. **182**, 1628–1644 (2010).
[21]M. Liberman, M. Ivanov, A. Kiverin, M. Kuznetsov, A. Chukalovsky, and T. Rakhimova, "Deflagration-to-detonation transition in highly reactive combustible mixtures," Acta Astronaut. **67**, 688–701 (2010).
[22]L. Kagan and G. Sivashinsky, "Parametric transition from deflagration to detonation: Runaway of fast flames," Proc. Combust. Inst. **36**, 2709–2715 (2017).
[23]A. Koksharov, V. Bykov, L. Kagan, and G. Sivashinsky, "Deflagration-to-detonation transition in an unconfined space," Combust. Flame **195**, 163–169 (2018).
[24]P. V. Gordon, L. Kagan, and G. Sivashinsky, "Parametric transition from deflagration to detonation revisited: Planar geometry," Combust. Flame **211**, 465–476 (2020).
[25]B. Deshaies and G. Joulin, "Flame-speed sensitivity to temperature changes and the deflagration-to-detonation transition," Combust. Flame **77**, 201–212 (1989).
[26]B.-T. Chu, "On the generation of pressure waves at a plane flame front," in *Symposium (International) on Combustion*, Vol. 4 (Elsevier, 1953) pp. 603–612.
[27]E. S. Oran, G. Chamberlain, and A. Pekalski, "Mechanisms and occurrence of detonations in vapor cloud explosions," Prog. Energy Combust. Sci. **77**, 100804 (2020).
[28]A. Y. Poludnenko, "Pulsating instability and self-acceleration of fast turbulent flames," Phys. Fluids **27**, 014106 (2015).
[29]A. Y. Poludnenko, T. A. Gardiner, and E. S. Oran, "Spontaneous transition of turbulent flames to detonations in unconfined media," Physical Review Letters **107**, 054501 (2011).
[30]J. Chambers, H. M. Chin, A. Y. Poludnenko, V. N. Gamezo, and K. A. Ahmed, "Spontaneous runaway of fast turbulent flames for turbulence-induced deflagration-to-detonation transition," Physics of Fluids **34**, 015114 (2022).
[31]W. Rakotoarison, B. Maxwell, A. Pekalski, and M. I. Radulescu, "Mechanism of flame acceleration and detonation transition from the interaction of a supersonic turbulent flame with an obstruction: Experiments in low pressure propane–oxygen mixtures," Proceedings of the Combustion Institute **37**, 3713–3721 (2019).
[32]W. Rakotoarison, A. Pekalski, and M. I. Radulescu, "Detonation transition criteria from the interaction of supersonic shock-flame complexes with different shaped obstacles," Journal of Loss Prevention in the Process Industries **64**, 103963 (2020).
[33]B. Savard, E. R. Hawkes, K. Aditya, H. Wang, and J. H. Chen, "Regimes of premixed turbulent spontaneous ignition and deflagration under gas-turbine reheat combustion conditions," Combustion and Flame **208**, 402–419 (2019).
[34]R. Hytovick, J. Chambers, H. Chin, V. N. Gamezo, A. Poludnenko, and K. Ahmed, "The evolution of fast turbulent deflagrations to detonations," Physics of Fluids **35** (2023), 10.1063/5.0144663, 046112.
[35]H. Yang and M. I. Radulescu, "Dynamics of cellular flame deformation after a head-on interaction with a shock wave: reactive Richtmyer–Meshkov instability," Journal of Fluid Mechanics **923** (2021).
[36]L. Kagan, M. Liberman, and G. Sivashinsky, "Detonation initiation by a hot corrugated wall," Proc. Combust. Inst. **31**, 2415–2420 (2007).
[37]M. Liberman, A. Kiverin, and M. Ivanov, "On detonation initiation by a temperature gradient for a detailed chemical reaction models," Physics Letters A **375**, 1803–1808 (2011).
[38]M. Peswani and B. Maxwell, "Detonation wave diffraction in stoichiometric c 2 h 4/o 2 mixtures using a global four-step combustion model," Physics of Fluids **34**, 106104 (2022).
[39]C. Strozzi, A. Mura, J. Sotton, and M. Bellenoue, "Experimental analysis of propagation regimes during the autoignition of a fully premixed methane–air mixture in the presence of temperature inhomogeneities," Combustion and Flame **159**, 3323–3341 (2012).
[40]O. Schulz and N. Noiray, "Combustion regimes in sequential combustors: Flame propagation and autoignition at elevated temperature and pressure," Combustion and Flame **205**, 253–268 (2019).
[41]R. Mével, J. Sabard, J. Lei, and N. Chaumeix, "Fundamental combustion properties of oxygen enriched hydrogen/air mixtures relevant to safety analysis: Experimental and simulation study," Int. J. Hydrogen Energy **41**, 6905–6916 (2016).
[42]M. Reynaud, F. Virot, and A. Chinnayya, "A computational study of the interaction of gaseous detonations with a compressible layer," Phys. Fluids **29**, 056101 (2017).
[43]S. Taileb, J. Melguizo-Gavilanes, and A. Chinnayya, "Influence of the chemical modeling on the quenching limits of gaseous detonation waves confined by an inert layer," Combust. Flame **218**, 247–259 (2020).
[44]A. Suresh and H. T. Huynh, "Accurate monotonicity-preserving schemes with Runge–Kutta time stepping," J. Comput. Phys. **136**, 83–99 (1997).
[45]D. Kassoy, "The zeldovich spontaneous reaction wave propagation concept in the fast/modest heating limits," Journal of Fluid Mechanics **791**, 439–463 (2016).
[46]R. W. Houim and R. T. Fievisohn, "The influence of acoustic impedance on gaseous layered detonations bounded by an inert gas," Combustion and Flame **179**, 185–198 (2017).
[47]M. Reynaud, S. Taileb, and A. Chinnayya, "Computation of the mean hydrodynamic structure of gaseous detonations with losses," Shock Waves **30**, 645–669 (2020).
[48]J. Shepherd, "Detonation waves and propulsion," in *Combustion in high-speed flows*, edited by J. Buckmaster, T. L. Jackson, and A. Kumar (Springer, B.V, 1994) p. 373.
[49]J. Bdzil, "Steady-state two-dimensional detonation," Journal of Fluid Mechanics **108**, 195–226 (1981).
[50]G. R. Parker, E. M. Heatwole, M. D. Holmes, B. W. Asay, P. M. Dickson, and J. M. McAfee, "Deflagration-to-detonation transition in hot hmx and hmx-based polymer-bonded explosives," Combustion and flame **215**, 295–308 (2020).
[51]A. M. Khokhlov and E. S. Oran, "Numerical simulation of detonation initiation in a flame brush: the role of hot spots," Combust. Flame **119**, 400–416 (1999).
[52]V. N. Gamezo, A. M. Khokhlov, and E. S. Oran, "The influence of shock bifurcations on shock-flame interactions and ddt," Combust. Flame **126**, 1810–1826 (2001).

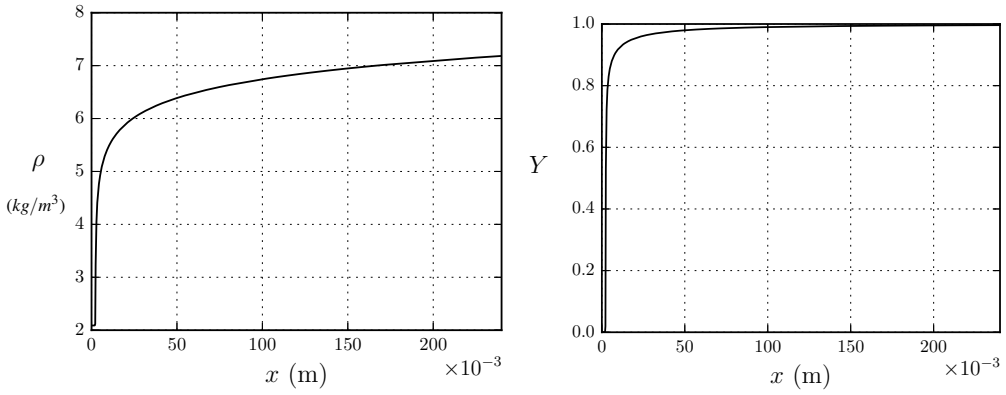

FIG. 18. Density field set as initial condition for 1-D propagating reactive wave - $\alpha = \pi$.

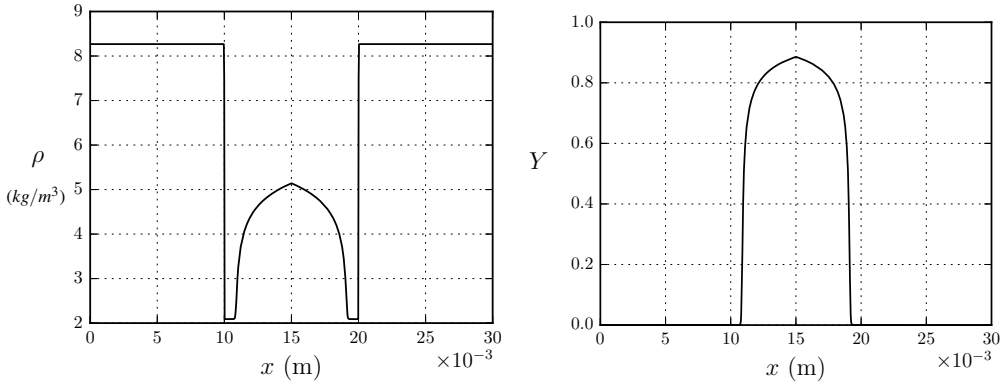

FIG. 19. Density field set as initial condition for 1-D collision of plane reactive waves - $\alpha = 0$.

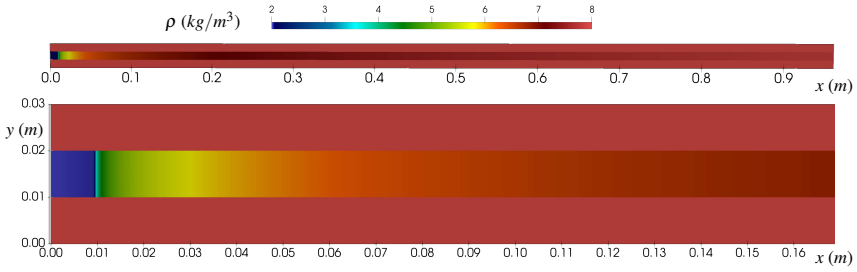

FIG. 20. Density field set as initial condition for propagating reactive wave - $\alpha = \pi$. Full 2-D domain (top) and zoom around the reactive wave (bottom).

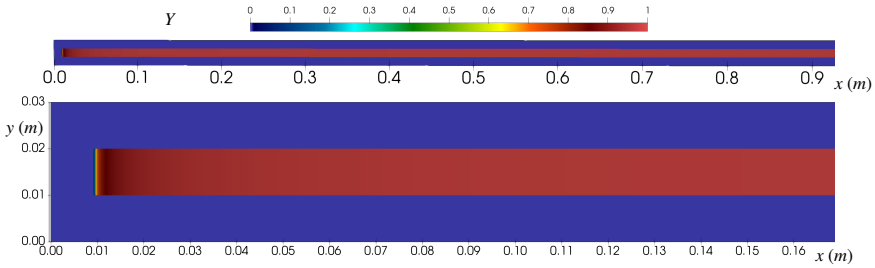

FIG. 21. Field of mass fraction of fresh reacting gas set as initial condition for propagating reactive wave - $\alpha = \pi$. Full 2-D domain (top) and zoom around the reactive wave (bottom).

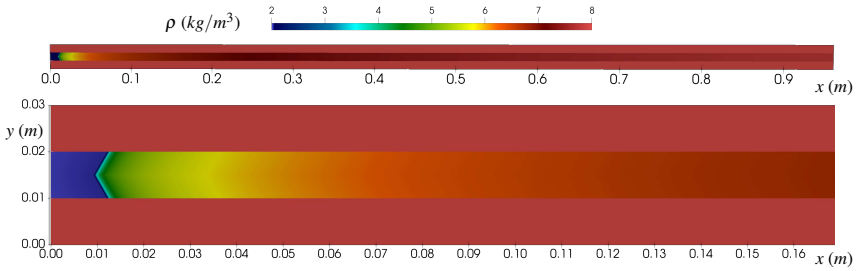

FIG. 22. Density field set as initial condition for obtuse-angle 2-D collision of reactive waves - $\alpha = 2\pi/3$. Full 2-D domain (top) and zoom around the reactive wave (bottom).

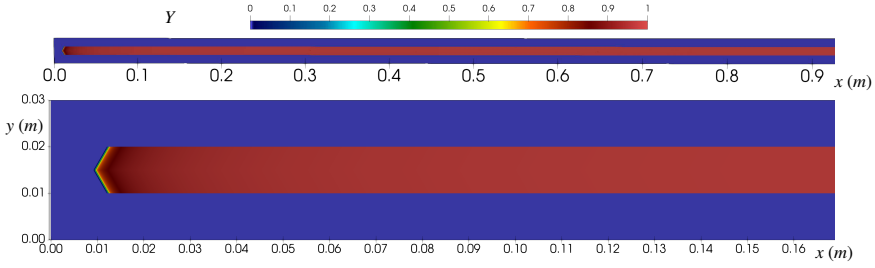

FIG. 23. Field of mass fraction of fresh reacting gas set as initial condition for obtuse-angle 2-D collision of reactive waves - $\alpha = 2\pi/3$. Full 2-D domain (top) and zoom around the reactive wave (bottom).

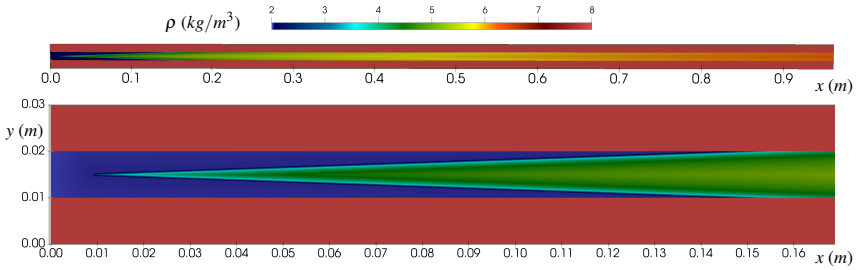

FIG. 24. Density field set as initial condition for acute-angle 2-D collision of reactive waves - $\alpha = \pi/45$. Full 2-D domain (top) and zoom around the reactive wave (bottom).

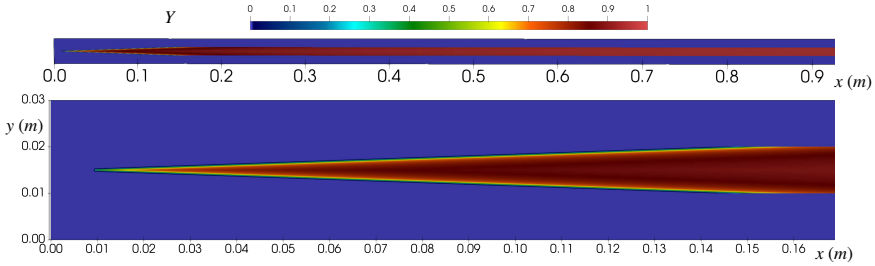

FIG. 25. Field of mass fraction of fresh reacting gas set as initial condition for acute-angle 2-D collision of reactive waves - $\alpha = \pi/45$. Full 2-D domain (top) and zoom around the reactive wave (bottom).

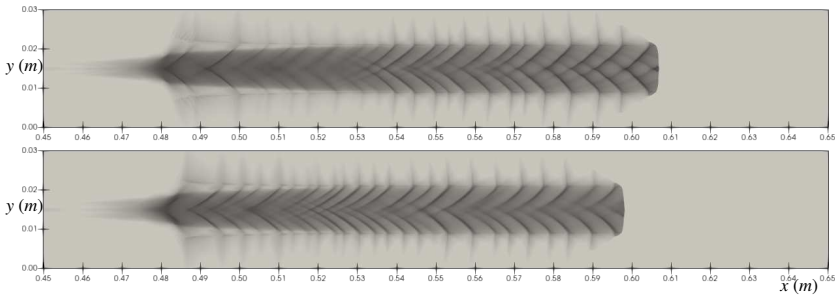

FIG. 26. Numerical soot foil obtained with the celle size $\Delta = 0.1\,\text{mm}$ (bottom) and $\Delta = 0.05\,\text{mm}$ (top) for $\alpha = \pi/45$.

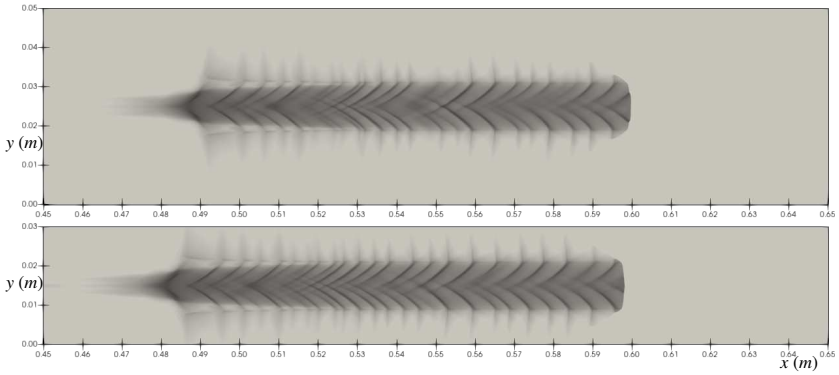

FIG. 27. Numerical soot foil obtained with passive layers of thickness 10 mm (bottom) and 20 mm (top) - $\alpha = \pi/45$.